13430–13439 *Nucleic Acids Research, 2014, Vol. 42, No. 21* *Published online 11 November 2014*
doi: 10.1093/nar/gku1135

Structural insights into the function of a unique tandem GTPase EngA in bacterial ribosome assembly

Xiaoxiao Zhang†, Kaige Yan†, Yixiao Zhang, Ningning Li, Chengying Ma, Zhifei Li, Yanqing Zhang, Boya Feng, Jing Liu, Yadong Sun, Yanji Xu, Jianlin Lei* and Ning Gao*

Ministry of Education Key Laboratory of Protein Sciences, Center for Structural Biology, School of Life Sciences, Tsinghua University, Beijing 100084, China

Received August 11, 2014; Revised October 23, 2014; Accepted October 24, 2014

ABSTRACT

Many ribosome-interacting GTPases, with proposed functions in ribosome biogenesis, are also implicated in the cellular regulatory coupling between ribosome assembly process and various growth control pathways. EngA is an essential GTPase in bacteria, and intriguingly, it contains two consecutive GTPase domains (GD), being one-of-a-kind among all known GTPases. EngA is required for the 50S subunit maturation. However, its molecular role remains elusive. Here, we present the structure of EngA bound to the 50S subunit. Our data show that EngA binds to the peptidyl transferase center (PTC) and induces dramatic conformational changes on the 50S subunit, which virtually returns the 50S subunit to a state similar to that of the late-stage 50S assembly intermediates. Very interestingly, our data show that the two GDs exhibit a pseudo-two-fold symmetry in the 50S-bound conformation. Our results indicate that EngA recognizes certain forms of the 50S assembly intermediates, and likely facilitates the conformational maturation of the PTC of the 23S rRNA in a direct manner. Furthermore, in a broad context, our data also suggest that EngA might be a sensor of the cellular GTP/GDP ratio, endowed with multiple conformational states, in response to fluctuations in cellular nucleotide pool, to facilitate and regulate ribosome assembly.

INTRODUCTION

The ribosome is a universal molecular machine responsible for protein biosynthesis in all living cells. Similar as protein translation, the assembly of ribosome from individual RNA and protein components *in vivo* is also an energetically expensive process, which requires a large number of functionally diverse factors (1,2), including multiple ATP-dependent RNA helicases and GTPases (3,4). In *Escherichia coli*, there are six GTPases (Era, RsgA, ObgE, YihA, YchF and EngA) reported to be involved in ribosome assembly [reviewed in (5)]. Most of these assembly GTPases are essential for cell growth and genetic perturbation of their genes confers generally similar phenotype, with defects in ribosomal subunit assembly and rRNA processing (1,4,5). However, it is not clear how these GTPases function at molecular level. A common feature of these assembly GTPases is that compared with translational GTPases, they have a low affinity for nucleotides (K_d in micromolar range) and a fast guanosine-5'-triphosphate/guanosine-5'-diphosphate (GTP/GDP) exchange rate, and are therefore proposed to be capable of sensing cellular energy level (GTP/GDP ratio) and couple ribosome assembly to various growth-control pathways (4).

Among these assembly GTPases, EngA (also known as Der, double-Era-like domains) is one of a kind, as it contains two tandemly arranged GTPase domains (GD1 and GD2, from the N- to C-terminus) (6,7). The first evidence implicating EngA in ribosome assembly is the observation that overexpression of EngA rescues ribosome profile abnormality in a Δ*rrmJ* (methyltransferase of U2552 of the 23S rRNA) strain (8). Further characterization reveals that EngA cofractionates primarily with the 50S subunit and depletion of EngA causes accumulation of rRNA precursors (9) and immature large ribosomal subunits that are missing several ribosomal proteins (L16, L27 and L36 in *Bacillus subtilis*; L9 and L18 in *E. coli*) (9,10,11), as well as a few other phenotypes associated with defects in ribosome biogenesis (12). The C-terminal sequences of EngA form an RNA-binding K Homology domain (KH domain) (13,14), which is important for both the 50S subunit interaction and the assembly function (15,16,17). Furthermore, the overall conformation of EngA (14), as well as its specificity to different ribosomal fractions (15,17,18) appears to be fine-

*To whom correspondence should be addressed. Tel: +86 01062794277; Fax: +86 01062771145; Email: ninggao@tsinghua.edu.cn
Correspondence may also be addressed to Jianlin Lei. Tel: +86 01062797699; Fax: +86 01062771145; Email: jllei@tsinghua.edu.cn
†The authors wish it to be known that, in their opinion, the first two authors should be regarded as Joint First Authors.
Present Address: Jing Liu, Shishi High School, Chengdu, Sichuan 610041, China.

tuned by nucleotide-binding states of its two GDs. Since the two GDs of EngA differ in nucleotide affinity (18,19,20) and GTP-hydrolyzing activity (11,13,20), EngA could be an ideal effector protein that is able to sense a wide-range change of the GTP/GDP ratio in the cell. Owing to this unique property, attempts using EngA as an anti-bacterial target have been underway (21,22).

In the present study, we solve the structure of EngA bound to the 50S subunit in the presence of GMPPNP using cryo-electron microscopy (cryo-EM). Our results show that EngA binds to the intersubunit face of the 50S subunit, embedded deeply inside the tRNA passage, with its KH domain interacting with the peptidyl transferase center (PTC) of the 50S subunit. Upon the binding of EngA, the 50S subunit undergoes large structural rearrangement, resulting in mobilization of helices 68–71 and loss of protein L33. Our structural data, together with previous genetic and biochemical data, suggest that the molecular role of EngA in ribosome assembly is to facilitate time-consuming assembly of the rRNA helices at the PTC. Interestingly, our data also indicate that the two GDs of EngA display a pseudo-two-fold symmetry, manifesting an unusual GTPase activation mechanism which likely relies on the dimeric configuration of the two GDs. These structural information has paved way for further functional and mechanistic dissection of EngA and potentially, to make use of its unique properties in anti-bacteria drug discovery.

MATERIALS AND METHODS

Protein preparation

The gene for EngA was cloned from *E. coli* DH5α strain using a standard Polymerase Chain Reaction (PCR). The PCR product was inserted into the expression cassette of the plasmid pET28a (Novagen). For site-directed mutations (H147A, R149E, E271K, K272E, R403E/R404E, R404E and R443E), pET28a-*engA* was used as PCR template and mutations were introduced in respective primers. PCR products containing mutations were digested with DpnI (New England Biolabs) to remove the template. A C-terminus deletion mutant (Δ464–490) was similarly obtained. Wild-type and mutant EngA constructs were transformed into *E. coli* BL21 (DE3) cells for overexpression. Cells were grown at 37°C in LB medium until OD600 reached ∼0.8. The overexpression was induced by 0.5 mM IPTG (isopropyl-β-D-thiogalactopyranoside) at 30°C for 7 h. Cells were collected by centrifugation at 5000 *g* (Avanti J-26 XP, JLA10.500 rotor, Beckman Coulter) for 10 min and disrupted by sonication (Ultrasonic cell crusher, Nanjing Xinchen Biotechnology) in lysis buffer (20 mM Tris–HCl, pH 7.5, 400 mM NH_4Cl). Cell lysates were clarified by centrifugation at 13 000 rpm (Avanti J-26 XP, JA25.50 rotor, Beckman Coulter) for 1 h. The supernatants were loaded onto a Ni-NTA column (Ni Sepharose 6 Fast Flow, GE healthcare) and eluted using elution buffer (20 mM Tris–HCl, pH 7.5, 400 mM NH_4Cl, 250 mM imidazole). Fractions of His-tagged EngA were pooled and concentrated to ∼1 ml. His-tagged proteins were incubated with Thrombin (Sigma, T4648) at 4°C overnight to remove the N-terminal His-tag. Proteins were reloaded onto a Ni-NTA column (Ni Sepharose 6 Fast Flow, GE healthcare), and the flow-through were collected. Proteins were further purified using an ion exchange column (Resource Q, GE healthcare) in a linear salt gradient (20 mM Tris–HCl, pH 7.5, 100 to 1000 mM NH_4Cl) and a gel filtration column (Superdex 200 column 10/300 GL, GE healthcare) equilibrated in storage buffer (20 mM Tris–HCl, pH 7.5, 400 mM NH_4Cl, 2 mM DTT). Purified proteins were stored at −80°C.

50S subunit purification

Ribosomes in all experiments were separated from the *E. coli* DH5α strain. Cells grown in fresh LB medium were harvested by centrifugation at 5000 *g* for 10 min (Avanti J-26 XP, JLA10.500 rotor, Beckman Coulter) and washed using resuspension buffer (10 mM Tris–HCl, pH 7.5, 100 mM NaCl). Resuspended cells were disrupted in opening buffer (20 mM Tris–HCl, pH 7.5, 500 mM NH_4Cl, 10 mM $Mg(OAc)_2$, 0.5 mM EDTA, 1 mM TCEP), and clarified by centrifugation at 13 000 rpm (Avanti J-26 XP, JA25.50 rotor, Beckman Coulter) for 1 h. The supernatant was transferred onto a 5-ml sucrose cushion (20 mM Tris–HCl, pH 7.5, 500 mM NH_4Cl, 0.5 mM EDTA, 10 mM $Mg(OAc)_2$, 33% sucrose, 1 mM TCEP) and centrifuged in a 70Ti rotor (Beckman Coulter) at 28 000 rpm for 18 h. The pellets were washed and dissolved in 2 ml opening buffer and subjected to another round of sucrose cushion-based centrifugation. The final pellets were dissolved in opening buffer and subjected to a 10–40% sucrose density gradient containing 15 mM $Mg(OAc)_2$ for 7 h at 30 000 rpm in a SW32 rotor (Beckman Coulter). Peak of 70S ribosomes was collected, concentrated and subjected to a 10–40% sucrose density gradient containing 2 mM $Mg(OAc)_2$ for 7 h at 30 000 rpm in a SW32 rotor (Beckman Coulter). Peaks of the 50S and 30S subunits were separately collected and concentrated.

GTPase activity assay

GTPase activities were measured using a NADH-coupled enzyme assay (23). The reaction buffer contained 50 mM MOPS, 300 mM KOAc,1 mM $Mg(OAc)_2$,1 mM phosphoenolpyruvate (Sigma, P0564), 0.4 mM NADH (Sigma, N8129), 1 mM GTP (Sigma, G8877), 20 U/ml lactic dehydrogenase (Sigma, L7525) and 15 U/ml pyruvate kinase (Sigma, P1506). EngA (3 μM) in the absence or presence of the 50S subunit (0.5 μM) were mixed in a 200-μl reaction buffer inside a 96-well plate kept at 37°C. Control experiments with the buffer, bovine serum albumin, plasmid DNA or the 50S alone were carried out similarly. The reactions were monitored continuously at a wavelength of 340 nm using a multifunctional fluorescent analyzer (FLUOstar Omega, BMG LABTECH). The linear ranges of the NADH-absorbance spectra over time were used for estimation of GTP hydrolysis rates. The velocity of the decline at 340 nm absorbance (AU340/min) were converted into the actual velocity of GTP hydrolysis (min^{-1}), based on a pre-measured standard concentration curve of NADH. Three independent measurements were performed to calculate the means and standard deviations.

Co-sedimentation assay

The 50S subunit (30 pmol) and the WT (600 pmol, both the His-tag containing or tag-free versions) or mutant EngA (600 pmol, tag-free) in the absence or presence of nucleotides (GTP, GDP or GMPPNP, ∼ 1 μmol) were incubated in 100-μl buffer (20 mM Tris–HCl, pH 7.5, 120 mM NH_4Cl, 2 mM $MgCl_2$) at 37°C for 15 min. The mixtures were then centrifuged at 10 000 *g* for 10 min to remove possible aggregates. The supernatants were carefully transferred onto a 90-μl sucrose cushion (20 mM Tris–HCl, pH 7.5, 120 mM NH_4Cl, 2 mM $MgCl_2$, 33% sucrose) and centrifuged using a TLA100 rotor (Beckman Coulter) at 95 000 rpm for 2 h. The pellets were dissolved in 15 μl buffer containing 20 mM Tris–HCl (pH 7.5), 120 mM NH_4Cl and 10 mM $MgCl_2$. One-third of total pellets and 1/36 of total supernatants were examined by 15% sodium dodecyl sulfate-polyacrylamide gel electrophoresis (SDS-PAGE).

Preparation of the 50S complexes and cryo-electron microscopy

The 50S subunit (∼60 nM) was incubated with His-EngA (1.8 μM) in the presence of GMPPNP (∼180 μM) in binding buffer (20 mM Tris–HCl, pH 7.5, 120 mM NH_4Cl, 10 mM $MgCl_2$) at 37°C for 15 min. The mixtures were centrifuged at 10 000 *g* for 10 min (Heraeus Fresco 21 centrifuge, Thermo scientific) to remove possible aggregates. Aliquots (4 μl) of the supernatants were applied to 300-mesh glow-discharged Quantifoil grids (Quantifoil Micro Tools GmbH). The grids were pre-coated with a thin layer of freshly made carbon film. FEI Vitrobot Mark IV was used for cryo-plunging. The images were collected using an FEI Titan Krios equipped with an FEI Eagle 4K × 4K CCD camera at 75 000× magnification. All images were collected under low dose condition (∼20 $e^-/Å^2$), with the AutoEMation software package (24).

Image processing

Preprocessing of micrographs and particle picking were performed using the SPIDER software package (25). For the 50S·EngA complex, 13 646 micrographs were collected and 6333 were kept. A total of 390 563 particles were obtained and used for the three-dimensional (3D) classification by the RELION software package (26). Particles were split into five classes, and 2 classes (189 614 particles) were combined for further structural refinement, based on the results of the 3D classification (Supplementary Figure S1). The refinement was done using the 3D auto-refine module of the RELION package. The final resolutions of the 50S·EngA map, are 5.0 and 6.5 Å (Supplementary Figure S2), according to the gold-standard Fourier Shell Correlation (FSC) 0.143 and 0.5 criteria (27), respectively. Postprocessing of the density map was done by RELIOIN, which included a B-factor-based sharpening. Local-resolution map was constructed using the software ResMap (28).

Atomic model building and flexible fitting

Atomic model of *E. coli* EngA was modeled using I-TASSER (29), using the crystal structures of *Thermotoga maritima* and *B. subtilis* EngA (13,14) as templates. The resulting atomic model of the full-length (490 residues) EngA was manually docked into the density map using Chimera (30). Sequences that were modeled without homology models were examined carefully in the density map. As a result, some sequences with unreliable coordinates were removed from further analysis, including residues 29–39 (Switch I of GD1), 57–64 (part of GD1 Switch II), 170–194 (GD1-GD2 linker) and 463–490 (C-terminal extension). The resulting atomic model of EngA, together with a previously published model for the 50S subunit (PDB ID: 2WWQ) (31), were docked into the density map and optimized using a flexible fitting approach based on molecular dynamics simulation (32). After flexible fitting, temperature map of the 50S·EngA structure was constructed using an extension module (rmsd_b.py and color_b.py, http://pldserver1.biochem.queensu.ca/_rlc/work/pymol/) of PyMol (http://www.pymol.org), in a way as previously described (33). The 23S rRNA in the 50S·EngA structure was colored based on the 3D distance deviation from the 23S rRNA in a 70S ribosome (PDB ID: 2WWQ) (31). PyMOL and Chimera were used for structural analysis and figure preparation.

RESULTS

Overview of the cryo-EM structure of the 50S·EngA complex

To optimize the cryo-EM sample preparation, we first tested the binding of EngA to the 50S subunit in the presence of different nucleotides, using a co-sedimentation assay. Consistent with previous observations (9,18), EngA in the GMPPNP-bound state shows the highest affinity for the 50S subunit (Supplementary Figure S3). The *in vitro* assembled 50S·EngA complex was subjected to cryo-EM single particle analysis, and as a result, a density map for the 50·EngA complex was obtained at near atomic resolution (5.0 Å) (Supplementary Figure S2). Very interestingly, in the cryo-EM structure (Figure 1), EngA is deeply embedded inside the tRNA passage on the 50S subunit, occupying the space of the P-site and E-site tRNAs (Figure 1D), with its C-terminal KH domain located at the PTC of the 23S rRNA. To facilitate quantitative structural analysis, a pseudo-atomic model was built using a flexible fitting approach (32). The nicely resolved secondary structural features in the density map greatly facilitated the modeling (Figure 1C, Supplementary Movies S1 and S2). The detailed interactions of EngA with the 50S subunit and their functional implications are discussed in the following sections.

EngA interacts with the ribosomal PTC

In the 50S·EngA complex, all three domains of EngA make extensive contacts with the 50S subunit. The EngA-GD1 interacts with H82, H88 and L1 (Figure 2A), which are all ribosomal components involved in the E-site tRNA interactions. The EngA-GD2 sits underneath the largely displaced H68, interacting with several surrounding rRNA helices, including H68, H88 and H75 (Figure 2B). In addition, a 50S protein L2 is near the interface between EngA-GD2 and

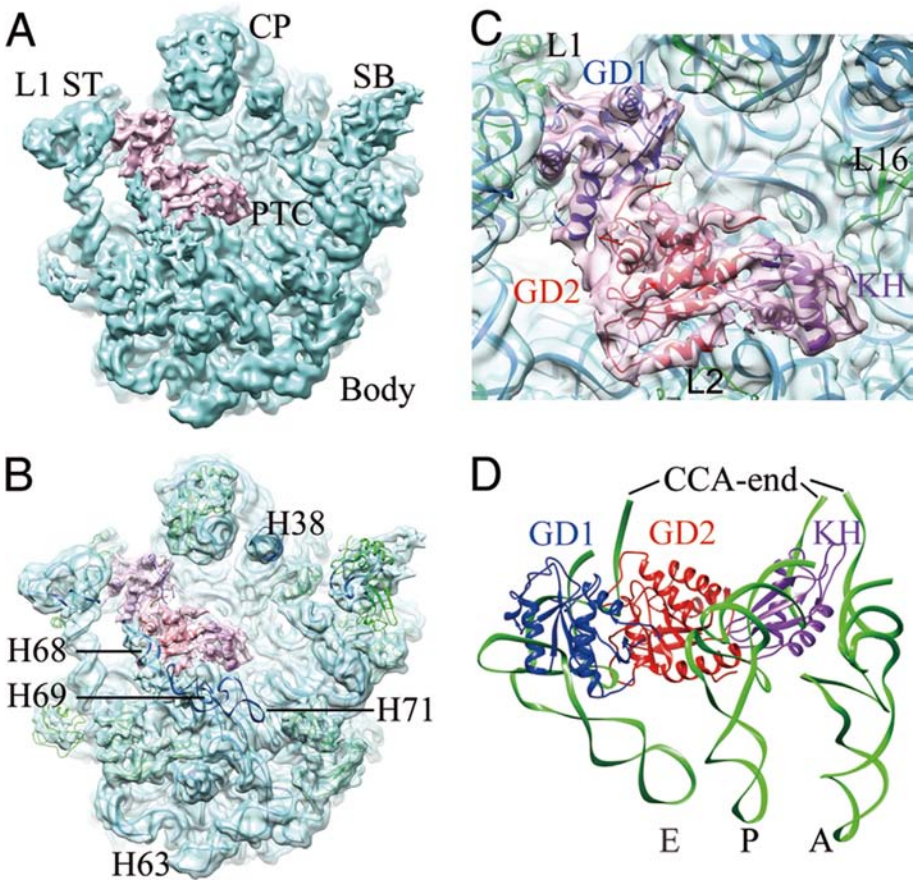

Figure 1. Overview of the cryo-EM structure of the 50S·EngA complex. (**A**, **B** and **C**). Surface representation of the cryo-EM density map of the 50S·EngA complex, with flexibly fitted atomic model superimposed (B and C). L1 ST, L1 stalk; CP, central protuberance; SB, L7/L12 stalk base; PTC, peptidyl transferase center. (**D**) Comparison of EngA with tRNAs on the 50S subunit. Atomic model of EngA in the 50S·EngA complex is superimposed with structures of the three tRNAs (E-, P- and A-site) on the 70S ribosome. The coordinates of tRNAs are from a previous publication (PDB ID: 2WDK). Structural alignment was done using the 50S subunit as reference. The three domains of EngA, GD1, GD2 and KH, are colored blue, red and purple, respectively. The three tRNAs are colored green, with CCA ends labeled.

H75. The most insightful finding comes from the KH domain of EngA, as it shows strong interactions with the components from the PTC, such as H93 and H80 (Figure 2C). The KH domain contains a large number of highly conserved basic residues (arginine or lysine), and most of them are located at the interface between the PTC and the KH domain (Figure 2D). Notably, EngA has a species-specific extension at its very C-terminus (residues 463 to 490 in *E. coli*) (15), which was not resolved in our cryo-EM density map. Given the location of the KH domain at the PTC (Figure 2D), this C-terminal extension of EngA could have potential interactions with the PTC helices and L16 in its proximity.

Specific mutations at the 50S:EngA interface impairs EngA binding

To validate the atomic interactions inferred from structural data, we designed point mutations and examined the binding of EngA mutants to the 50S subunit. According to both structural information and sequence data (Supplementary Figure S4), a few point mutations, namely, H147A and R149E at GD1, E271K and K272E at GD2, R403E, R404E and R443E at the KH domain, as well as a C-terminus truncated Δ464–490 mutant were constructed (Figure 3A). Firstly, H147 and R149 show direct interaction with H82 of the 23S rRNA, and H147 is highly conserved across species (Supplementary Figure S4). These two GD1 mutants showed significantly reduced binding to the 50S subunit (Figure 3B). Secondly, E271 (also conserved across species) and K272 are also in the proximity of the rRNA interface. These two GD2 mutations as well impaired factor binding, with E271K to be more defective, and K272E to be little to no effect (Figure 3B). This observation agrees with previous data that a mutant *E. coli* strain harboring E271K mutation has serious growth defect (34). Thirdly, R403, R404 and R443 are in the proximity of the interface, but not in close, direct contact with the rRNA. Results of the KH mutants showed that they had slightly reduced affinities for the 50S subunit (Figure 3B). However, none of them completely abolished the binding activity. These data indicate that the binding of the KH domain is a collective effort of multiple contributing basic residues, presumably to provide a general positively charged surface to the PTC. The last mutation is Δ464–490, which showed significantly reduced binding (Figure 3B), in concordance to previous re-

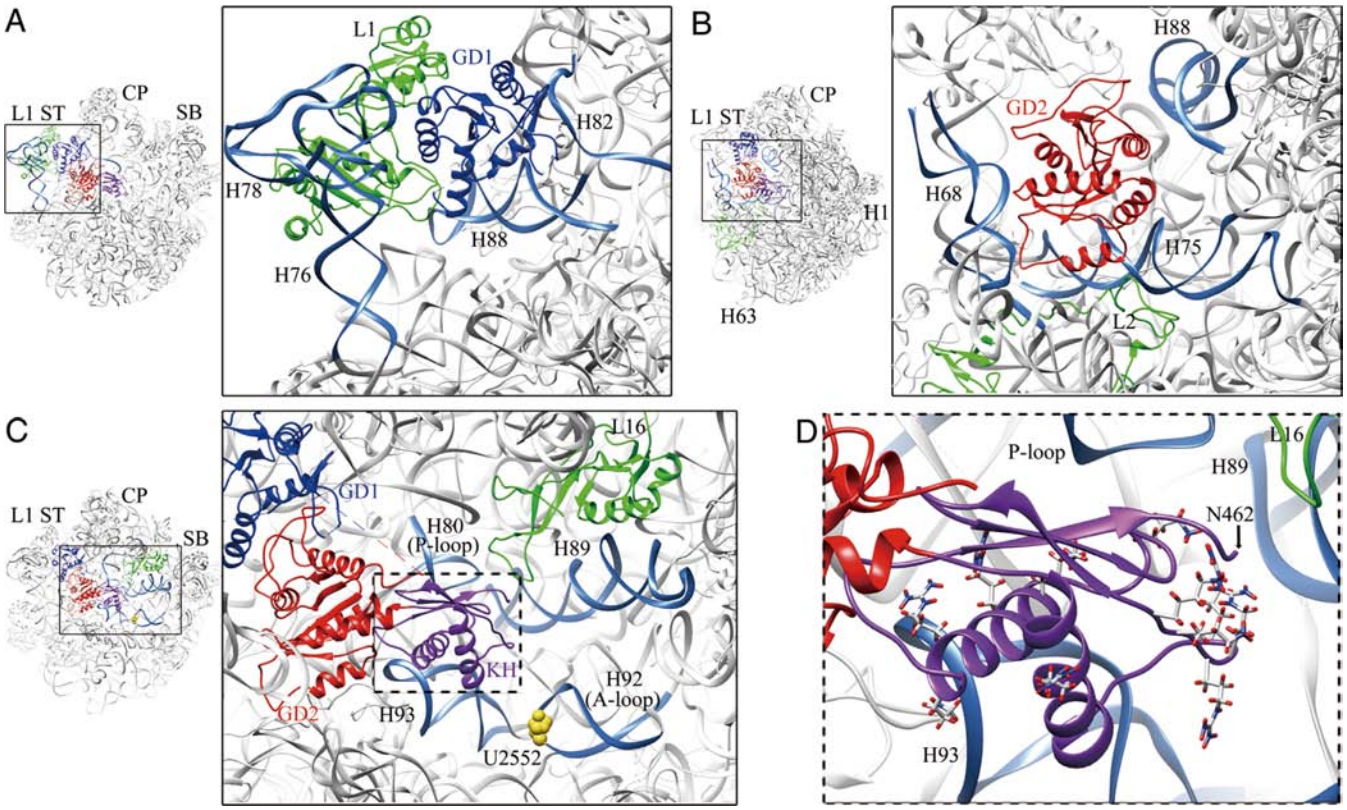

Figure 2. Detailed interactions of EngA with the 50S subunit in the 50S·EngA complex. (**A**) Interaction of the EngA-GD1 with protein L1, L1 stalk, H82 and H88 of the 23S rRNA. (**B**) Interactions of the EngA-GD2 with H68, H75 and H88 of the 23S rRNA, and possibly with protein L2. (**C**) KH domain is surrounded by helices from the PTC, including H80 (P-loop), H89, H92 (A-loop) and H93 of the 23S rRNA. (**D**) Zoom-in view showing strong polar interactions between the KH domain and the PTC helices. Positively charged residues (arginine and lysine) are displayed in stick models. GD1, GD2 and KH domain of EngA are painted in blue, red and purple, respectively. The U2552 of the A-loop (H92), the methylation site of RrmJ is shown in yellow ball representation. The C-terminal sequences beyond residue 462 were disordered in the cryo-EM map and therefore was not present in the model.

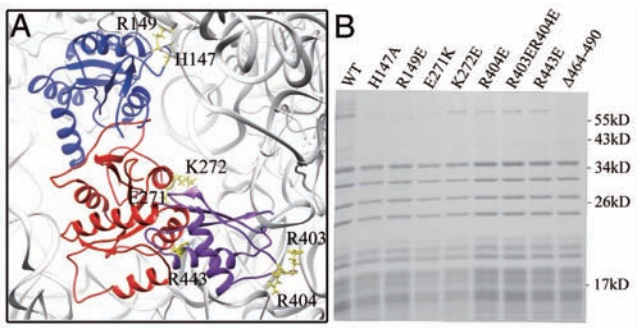

Figure 3. Specific mutations impairs binding of EngA to the 50S subunit. (**A**) The structure of EngA in the 50S·EngA complex is shown in cartoon representation, with three domains GD1, GD2 and KH colored blue, red and purple, respectively. Selected residues for mutagenesis are displayed in yellow stick models. (**B**) The WT (wild type) and mutant EngA binding to the 50S subunits, in the presence of saturating GMPPNP, were examined by co-sedimentation assay. The expression His-tags in these proteins were removed by thrombin. The pellets were resolved by SDS-PAGE. The band of EngA is above the 55 kD marker.

port that C-terminal extension deletion is not functional *in vivo* (16).

With all these mutational data, it appears that the KH domain interacts, through multiple basic residues, with the 50S subunit extensively. In contrast, GD1 (H147A and R149E) appears to interact in a more sequence-specific way with the 50S subunit. Notably, this is in consistent with previous data suggesting that GD1 controls the binding specificity of EngA to different ribosomal fractions (18).

EngA binding induces large conformational changes on the 50S subunit

Upon EngA binding, the 50S subunit undergoes dramatic conformational changes at a number of locations. The most significant one lies at the rRNA helices 68–71, which are seen to be extensively displaced from their normal positions (Figures 1B, 4 and Supplementary Figures S5 and S6). Especially, H68, as a long helix that paves the tRNA passage from the PTC to the tRNA exit site, is in a floating position, which results in fragmentation of densities at the terminal half of its helix stem (Figure 4A and Supplementary Movie S1). Another major conformational change is that L1 stalk is in a closed position (Supplementary Figure S6A), resulted from a direct interaction between GD1 of EngA and protein L1 (Figure 2A). Furthermore, H38 and the stalk base of L7/L12 (H43–44) also deviate from their normal positions (Figure 4D and Supplementary Figure S6A). Apart from these large conformational changes, EngA induces a systematic rearrangement of rRNA helices

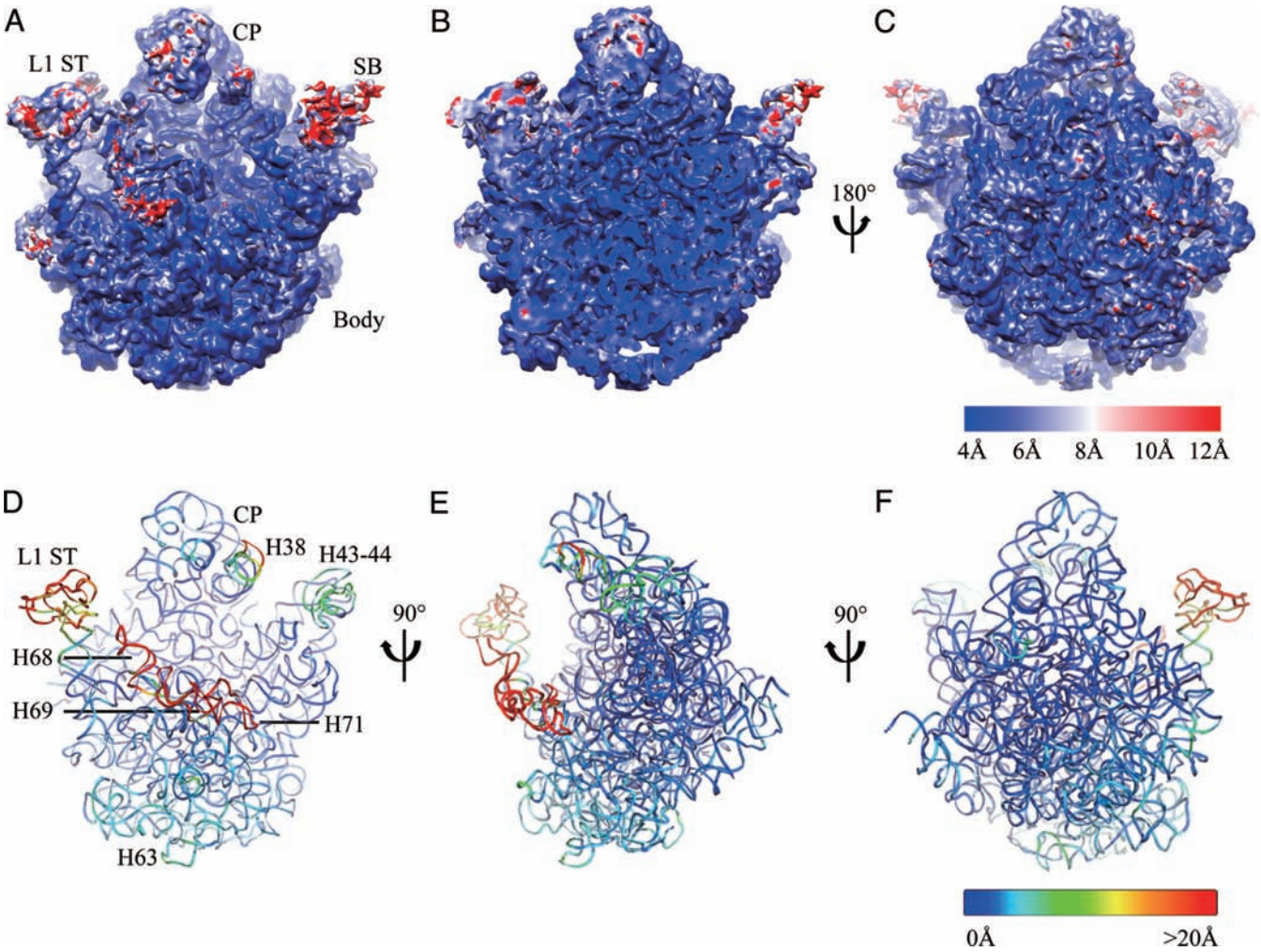

Figure 4. EngA induces dramatic conformational changes on the 50S subunit. (**A**, **B** and **C**) Surface and cross-section of the local resolution map of the 50S·EngA density map. Surface representation of the local resolution map, viewed from the intersubunit (A), solvent face (C) and in a cross section (B). The map is colored according to the scale bar. Landmarks of the 50S subunit are labeled: L1 ST, L1 stalk; SB, L7/L12 stalk base; CP, central protuberance. (**D**, **E** and **F**) Temperature map of the 23S rRNA in the 50S·EngA complex. The atomic model of the 23S rRNA in the 50S·EngA complex is colored based on its 3D distance deviation from that in a 70S ribosomal complex (PDB ID: 2WWQ) (31).

at the lower body of the 50S subunit, with a scale up to 5 Å (Figure 4D), compared with the structure of the 23S rRNA in a 70S ribosomal complex (31). Lastly, L33 is not present in the 50S·EngA complex, as it overlaps with the EngA-GD1 (Supplementary Figure S7), indicating that a competitive binding between EngA and L33 has driven the dissociation of L33.

The displacement of H68–71 in the 50S·EngA complex reminds us of our previous structures of the immature 45S subunits isolated from an assembly factor-deficient strain (35), which show that the docking of H68 is rate-limiting during the late-stage assembly of the 50S subunit. Together with observed steric clash between EngA and L33 (Supplementary Figure S7) and extensive structural rearrangement of the 23S rRNA upon EngA binding (Figure 4), it suggests that the binding of EngA has virtually returned the 50S subunit to a conformation that largely resembles the immature 45S subunits. Especially, the binding of EngA would prevent the 30S subunit association, since H69–71 is involved in the formation of several essential intersubunit bridges (36). Indeed, EngA inhibits the *in vitro* translation of a reporter mRNA in a dose-dependent manner (Supplementary Figure S8). Taking together, our data indicate that the native substrate of EngA is a certain form of assembly intermediate that is defective in subunit association and yet to be functionally active.

Pseudo-two-fold symmetric arrangement of two GDs on the 50S subunit

EngA adopts a fully extended conformation in the 50S·EngA complex. Very interestingly, the two GDs exhibit a pseudo-two-fold symmetry, with their switch regions facing each other in an antiparallel orientation (Figure 5A). Both nucleotide-binding pockets of EngA are distant from the ribosomal components, excluding a direct role of the 50S subunit in activating the GTPase of EngA in a similar way as it does on translational GTPases (37). To test whether the 50S subunit could stimulate the GTPase activ-

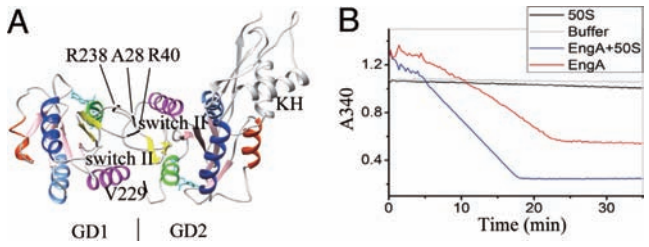

Figure 5. The 50S subunit stimulates the GTPase of EngA by juxtaposing GD1 and GD2 in a dimeric configuration. (**A**) Pseudo-two-fold symmetric arrangement of two GTPase domains in the 50S·EngA structure. Corresponding structural elements (α-helices and β-strands) in the two GTPase domains are separately colored. The bound nucleotides are displayed in stick models (cyan). Switch II regions of the two GTPase domains are colored magenta. The Switch I regions are largely disordered, and only the respective ends are shown in black (A28, R40, V229 and R238). (**B**) Experimental curves of the NADH-coupled GTPase assay, showing the time-course decline of A340 absorbance. In the presence of the 50S subunit, the GTPase activity of EngA is enhanced. Each measurement was repeated for three times, and for clarification, only one curve from them was shown.

ity of EngA, we measured the GTPase activities of wild-type EngA in the absence or presence of the 50S subunit, using a coupled enzyme assay (23). The reaction system contains a GTP regeneration system (see 'Materials and Methods' section), which enables a relatively longer linear range for accurate estimation of the apparent rates of GTP hydrolysis (Figure 5B). As a result, the measured basal GTPase level of EngA is relatively low, $\sim 3.35 +/- 0.02\ min^{-1}$, consistent with previous reports based on different approaches (11,21,38). While the 50S subunit alone shows virtually no enzymatic activity, addition of the 50S subunit to EngA results in a moderately enhanced GTPase activity by 1.4-fold. Although the stimulation by the 50S subunit seems to be small, a number of control experiments demonstrated that the observed GTPase activation is likely specific (Supplementary Figure S9), indicating that the 50S subunit is indeed the GAP (GTPase-activating protein) component of EngA. The moderate stimulation further suggests that the mature 50S subunit is not the native substrate of EngA and full stimulation might need a certain form of the 50S assembly intermediate.

Nucleotide-binding dependent conformational changes of EngA

Next, we compared the 50S-bound structure of EngA with two available crystal structures (*T. maritima* and *B. subtilis*) (13,14). The cryo-EM sample was prepared with a large excess of GMPPNP and therefore, the structure should reflect full occupancy of GMPPNP at both GD1 and GD2 nucleotide-binding sites. Structural alignment of the three structures using the KH and GD2 domains as reference reveals that GD2 and KH domain largely remain as a single rigid piece (Figure 6). But strikingly, an apparent motion of GD1 could be identified, with snapshots of GD1 in a continuous trajectory. Comparison of these different conformations indicates that GD2, together with KH domain as a structural unit, does not respond dramatically to its nucleotide-binding state (Figure 6). In contrast, binding of GMPPNP to GD1 greatly mobilizes GD1, resulting in a fully extended conformation. Consistently, these structural observations agree with previous biochemical data showing that GD1 regulates specificity of EngA in response to different nucleotides binding on the two GDs (18).

Altogether, the structural comparison indicates that EngA distinguishes itself from typical G-proteins by possessing more than two conformational states, and suggest that subtle changes in cellular guanine nucleotide pool might has a complex regulation on the structural dynamics of EngA.

DISCUSSION

EngA is a unique member of the GAD (GTPases activated by dimerization) family GTPases

This symmetric arrangement of GD1 and GD2 immediately suggests that the two enzymatic centers might work in a cooperative manner. In fact, the *in vivo* function of EngA requires the integrity of both GDs (9,11,16). Notably, previous *in vitro* biochemical analyses reveal that full-length EngA is likely in an auto-inhibitive conformation, and removal of the KH domain (38) or inactivation of GD2 by mutation in the NKXD G4 motif (13) results in increase of the overall basal GTPase activity. Together with our structural data, it indicates that the 50S subunit might reorganize the two GDs into a pseudo-dimeric conformation such that they might be mutually activated in a *trans* manner. The role of the 50S subunit, as a GAP for EngA, is highly likely achieved by the juxtaposition of GD1 and GD2 in an active conformation.

This distinctive arrangement of two GDs thus defines EngA as a unique member of the GAD (GTPases activated by dimerization) family GTPases (39,40). Notably, other translation-related GTPases are also found to be in the GAD family. For examples, signal recognition particle (SRP) and its receptor FtsY, also rely on the formation of heterodimer for their GTPase activation (41) on translating ribosomes. Another example is a phylogenetically conserved tRNA modification enzyme, MnmE, which instead forms a homodimer to activate its GTPase (42). Therefore, EngA represents a novel class of GAD that requires a pseudo-dimerization of two covalently connected GDs for activation.

Molecular role of EngA in ribosome assembly

In the present work, we characterize the structure of EngA bound to the 50S subunit in the presence of GMPPNP. The 50S subunit in the 50S·EngA structure is sharply different from its mature conformation, with a massive displacement of several central helices (H68–71), a dramatic inward movement of the L1 stalk, a systematic rearrangement of the lower body helices, and a depletion of protein L33. Many of these structural features were also found to be associated with *in vivo* immature 45S subunits (35). Therefore, these structural data are highly consistent with proposed role of EngA in ribosome assembly (4,9), and indicate that EngA·GTP recognizes a specific 50S assembly intermediate with defined protein composition and rRNA conformation during the *in vivo* assembly of the 50S subunit. Previously, we showed that the assembly of the PTC is relatively

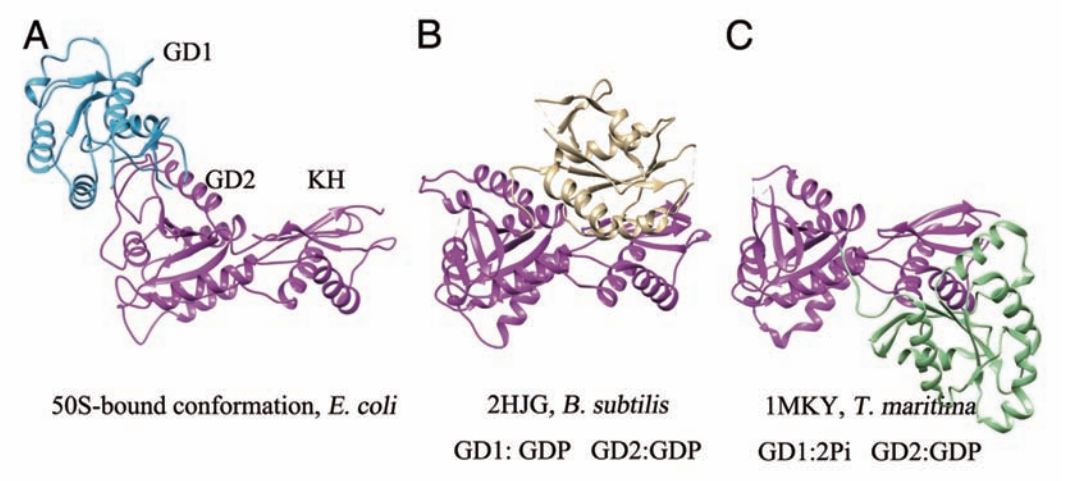

Figure 6. Conformational dynamics of EngA. (**A**) EngA in the 50S·EngA·GMPPNP complex. (**B**) The crystal structure of the *Bacillus subtilis* EngA in complexed with GDP (PDB ID: 2HJG) (14). Both nucleotide-binding sites are occupied by GDP. (**C**) The crystal structure of the *Thermotoga maritima* EngA (PDB ID: 1MKY) (13), with GDP bound to the nucleotide-binding site of GD2, and two phosphates to the nucleotide-binding site of GD1. The three structures are aligned using GD2 and KH domains as reference. GD1 domains of the three structures are differently colored.

late and it remains in a highly dynamic conformation in immature 45S subunits (35). The slow folding of the ribosomal PTC in the 45S subunit (35) and the specific interaction between EngA-KH and the PTC thus suggest that EngA likely has a direct role as an rRNA chaperone to facilitate tertiary rRNA interactions at the PTC. In fact, this view is supported by observed genetic interaction between EngA and RrmJ (8). RrmJ is a heat-shock methyltransferase of U2552 of the A-loop from the PTC (Figure 2C). Deletion of *rrmJ* causes a slow-growth phenotype and accumulation of defective 50S subunits in mutant cells (43,44). Since overexpression of EngA could suppress the phenotype of the Δ*rrmJ* strain, EngA likely contributes to reducing the flexibility of the PTC helices to facilitate their time-consuming assembly in a direct manner.

Furthermore, our structural data is consistent with another line of evidence that shows an interesting functional link between L9 and EngA. Firstly, depletion of EngA in *E. coli* results in loss of L9 in premature ribosomal particles (9). Secondly, L9 was recently found to be important for the cell fitness of two EngA mutant strains (E271K and T57I) (34), suggesting that there is, to a certain extent, a functional interplay between EngA and L9 in ribosome assembly. In the 50S·EngA structure, EngA causes a dramatic inward movement of L1 stalk, and L9 is exactly located at the root of L1 stalk, inserted into a helical junction. Therefore, the observed genetic interaction between EngA and L9 could be perfectly explained by the fact that both of them bind to a flexible element of the 23S rRNA and could affect the structural dynamics of L1 stalk during subunit assembly.

In summary, our structural data provides structural details for the primary function of EngA in ribosome biogenesis and suggests that the molecular role of EngA in the late-stage 50S subunit assembly is to stabilize certain forms of assembly intermediates to allow efficient and productive folding of the central helices of the 23S rRNA. Especially, EngA is incompatible with the mature conformation of helices 68–71, and by binding to the 50S subunit, it makes the 50S subunit apparently defective in subunit association. Notably, many other assembly factors seem to adopt a similar strategy in order to prevent premature association of subunits, e.g., by changing the conformation of rRNA helices involved in subunit association, such as Era (45), RbfA (46) and ObgE (47), or by directly blocking the intersubunit bridging contacts, such as RimM (33) and RsgA (48). Particularly, two 30S assembly factors, RbfA and KsgA, are capable of mobilizing a long rRNA helix (h44) on the mature 30S subunit (46,49) *in vitro*, in a similar fashion as EngA does to H68.

Possible role of EngA in cellular growth control during stress responses

It is known that cellular concentrations of different nucleotides, as a function of growth phase and metabolic state, play important roles in bacterial physiology. Functions of many ATPases and GTPases are strictly dependent on their bound nucleotides and particularly sensitive to the relative concentrations of different nucleotides in the cell. For example, a recently characterized ABC (ATP-binding cassette) protein in *E. coli*, EttA, is able to regulate translation elongation in response to the change in ATP/ADP ratio when cells enter long-term stationary phase (50,51). Ribosome biogenesis GTPases, endowed with low affinities for guanine nucleotides and fast GTP/GDP exchange rates, are also proposed to have regulatory roles in coupling ribosome assembly and translation cycle to various growth control pathways (1,3,4,5).

Consistent to this general view, EngA has been functionally linked to the stringent response pathway in *E. coli* (52), as well as other growth control related processes involving chromosome segregation, cell morphology and cell wall structure (7,53,54). The stringent response is a well-studied signal transduction system in bacteria and plants. Upon nutrition shortage, cells respond by a sharp increase of a

guanine-derivative molecule ppGpp, which has multiple cellular targets and especially, ppGpp acts as a cofactor for RNA polymerase complex (RNAP) to change the cellular transcriptional profile (55). Besides RNAP, ppGpp also targets multiple cellular GTPases (55), including IF2, EF-Tu, EF-G [(56) and reference therein] and ribosome assembly GTPases, such as ObgE [(47) and reviewed in (5)]. It was shown that overexpression of RelA, the enzyme responsible for ppGpp synthesis, rescues the growth defect of an EngA (N321D) mutant strain (52). Very recently, it was demonstrated that ppGpp binds to EngA with a similar affinity as GDP does (12). Since EngA, with its two GDs, is in principle an ideal sensor of cellular guanine nucleotide fluctuation, it might have a more general role as a master sensor of cellular energy status to regulate ribosome assembly, in parallel to other ppGpp-mediated processes to downregulate subunit production. A possible scenario is that cellular concentrations of guanine nucleotides and maturation states of the 50S precursors, along with other factors, such as a potential GAP (YihI) for EngA (38), determine the timing of the binding and departure of EngA in normal condition, and ppGpp could affect the binding or/and timely release of EngA so as to change the subunit production in response to nutrient availability. Nevertheless, this possible regulatory role of EngA still lacks molecular detail and awaits for further biochemical characterization.

ACCESSION NUMBERS

The density map of the 50S·EngA·GMPPNP complex has been deposited in the EMDataBank under accession code of 6149. The atomic model has been deposited in the Protein Data Bank under accession code of 3J8G.

SUPPLEMENTARY DATA

Supplementary Data are available at NAR Online.

ACKNOWLEDGEMENT

We acknowledge the China National Center for Protein Sciences (Beijing) and the 'Explorer 100' cluster system of Tsinghua National Laboratory for Information Science and Technology for providing computation resource.

FUNDING

National Natural Science Foundation of China [31422016, 31470722 to N.G.], Ministry of Science and Technology of China [2010CB912402, 2013CB910404 to N.G., 2010CB912401 to J.L.], Beijing Higher Education Young Elite Teacher Project [YETP0131 to N.G.]; Tsinghua University [20131089278 to N.G.]. Funding for open access charge: Ministry of Science and Techology of China [2010CB912402 to N.G.].
Conflict of interest statement. None declared.

REFERENCES

1. Shajani,Z., Sykes,M.T. and Williamson,J.R. (2011) Assembly of bacterial ribosomes. *Ann. Rev. Biochem.*, **80**, 501–526.
2. Wilson,D.N. and Nierhaus,K.H. (2007) The weird and wonderful world of bacterial ribosome regulation. *Crit. Rev. Biochem. Mol. Biol.*, **42**, 187–219.
3. Strunk,B.S. and Karbstein,K. (2009) Powering through ribosome assembly. *RNA*, **15**, 2083–2104.
4. Britton,R.A. (2009) Role of GTPases in bacterial ribosome assembly. *Ann. Rev. Microbiol.*, **63**, 155–176.
5. Verstraeten,N., Fauvart,M., Versees,W. and Michiels,J. (2011) The universally conserved prokaryotic GTPases. *Microbiol. Mol. Biol. Rev.*, **75**, 507–542, second and third pages of table of contents.
6. Caldon,C.E., Yoong,P. and March,P.E. (2001) Evolution of a molecular switch: universal bacterial GTPases regulate ribosome function. *Mol. Microbiol.*, **41**, 289–297.
7. Hwang,J. and Inouye,M. (2001) An essential GTPase, der, containing double GTP-binding domains from Escherichia coli and Thermotoga maritima. *J. Biol. Chem.*, **276**, 31415–31421.
8. Tan,J., Jakob,U. and Bardwell,J.C. (2002) Overexpression of two different GTPases rescues a null mutation in a heat-induced rRNA methyltransferase. *J.Bacteriol.*, **184**, 2692–2698.
9. Hwang,J. and Inouye,M. (2006) The tandem GTPase, Der, is essential for the biogenesis of 50S ribosomal subunits in Escherichia coli. *Mol. Microbiol.*, **61**, 1660–1672.
10. Schaefer,L., Uicker,W.C., Wicker-Planquart,C., Foucher,A.E., Jault,J.M. and Britton,R.A. (2006) Multiple GTPases participate in the assembly of the large ribosomal subunit in Bacillus subtilis. *J. Bacteriol.*, **188**, 8252–8258.
11. Bharat,A., Jiang,M., Sullivan,S.M., Maddock,J.R. and Brown,E.D. (2006) Cooperative and critical roles for both G domains in the GTPase activity and cellular function of ribosome-associated Escherichia coli EngA. *J. Bacteriol.*, **188**, 7992–7996.
12. Bharat,A. and Brown,E.D. (2014) Phenotypic investigations of the depletion of EngA in Escherichia coli are consistent with a role in ribosome biogenesis. *FEMS Microbiol. Lett.*, **353**, 26–32.
13. Robinson,V.L., Hwang,J., Fox,E., Inouye,M. and Stock,A.M. (2002) Domain arrangement of Der, a switch protein containing two GTPase domains. *Structure*, **10**, 1649–1658.
14. Muench,S.P., Xu,L., Sedelnikova,S.E. and Rice,D.W. (2006) The essential GTPase YphC displays a major domain rearrangement associated with nucleotide binding. *Proc. Natl. Acad. Sci. U.S.A.*, **103**, 12359–12364.
15. Tomar,S.K., Kumar,P., Majumdar,S., Bhaskar,V., Dutta,P. and Prakash,B. (2012) Extended C-terminus and length of the linker connecting the G-domains are species-specific variations in the EngA family of GTPases. *FEBS Open Bio*, **2**, 191–195.
16. Hwang,J. and Inouye,M. (2010) Interaction of an essential Escherichia coli GTPase, Der, with the 50S ribosome via the KH-like domain. *J. Bacteriol.*, **192**, 2277–2283.
17. Agarwal,N., Pareek,M., Thakur,P. and Pathak,V. (2012) Functional characterization of EngA(MS), a P-loop GTPase of Mycobacterium smegmatis. *PloS One*, **7**, e34571.
18. Tomar,S.K., Dhimole,N., Chatterjee,M. and Prakash,B. (2009) Distinct GDP/GTP bound states of the tandem G-domains of EngA regulate ribosome binding. *Nucleic Acids Res.*, **37**, 2359–2370.
19. Lamb,H.K., Thompson,P., Elliott,C., Charles,I.G., Richards,J., Lockyer,M., Watkins,N., Nichols,C., Stammers,D.K., Bagshaw,C.R. *et al.* (2007) Functional analysis of the GTPases EngA and YhbZ encoded by Salmonella typhimurium. *Protein Sci.*, **16**, 2391–2402.
20. Foucher,A.E., Reiser,J.B., Ebel,C., Housset,D. and Jault,J.M. (2012) Potassium acts as a GTPase-activating element on each nucleotide-binding domain of the essential Bacillus subtilis EngA. *PloS One*, **7**, e46795.
21. Bharat,A., Blanchard,J.E. and Brown,E.D. (2013) A high-throughput screen of the GTPase activity of Escherichia coli EngA to find an inhibitor of bacterial ribosome biogenesis. *J. Biomol. Screen.*, **18**, 830–836.
22. Comartin,D.J. and Brown,E.D. (2006) Non-ribosomal factors in ribosome subunit assembly are emerging targets for new antibacterial drugs. *Curr. Opin. Pharmacol.*, **6**, 453–458.
23. Ingerman,E. and Nunnari,J. (2005) A continuous, regenerative coupled GTPase assay for dynamin-related proteins. *Methods Enzymol.*, **404**, 611–619.
24. Lei,J. and Frank,J. (2005) Automated acquisition of cryo-electron micrographs for single particle reconstruction on an FEI Tecnai electron microscope. *J. Struct. Biol.*, **150**, 69–80.

25. Shaikh,T.R., Gao,H., Baxter,W.T., Asturias,F.J., Boisset,N., Leith,A. and Frank,J. (2008) SPIDER image processing for single-particle reconstruction of biological macromolecules from electron micrographs. *Nat. Protoc.*, **3**, 1941–1974.
26. Scheres,S.H. (2012) A Bayesian view on cryo-EM structure determination. *J. Mol. Biol.*, **415**, 406–418.
27. Henderson,R., Sali,A., Baker,M.L., Carragher,B., Devkota,B., Downing,K.H., Egelman,E.H., Feng,Z., Frank,J., Grigorieff,N. *et al.* (2012) Outcome of the first electron microscopy validation task force meeting. *Structure*, **20**, 205–214.
28. Kucukelbir,A., Sigworth,F.J. and Tagare,H.D. (2014) Quantifying the local resolution of cryo-EM density maps. *Nat. Methods*, **11**, 63–65.
29. Roy,A., Kucukural,A. and Zhang,Y. (2010) I-TASSER: a unified platform for automated protein structure and function prediction. *Nat. Protoc.*, **5**, 725–738.
30. Pettersen,E.F., Goddard,T.D., Huang,C.C., Couch,G.S., Greenblatt,D.M., Meng,E.C. and Ferrin,T.E. (2004) UCSF Chimera–a visualization system for exploratory research and analysis. *J. Comput Chem.*, **25**, 1605–1612.
31. Seidelt,B., Innis,C.A., Wilson,D.N., Gartmann,M., Armache,J.P., Villa,E., Trabuco,L.G., Becker,T., Mielke,T., Schulten,K. *et al.* (2009) Structural insight into nascent polypeptide chain-mediated translational stalling. *Science*, **326**, 1412–1415.
32. Trabuco,L.G., Villa,E., Mitra,K., Frank,J. and Schulten,K. (2008) Flexible fitting of atomic structures into electron microscopy maps using molecular dynamics. *Structure*, **16**, 673–683.
33. Guo,Q., Goto,S., Chen,Y., Feng,B., Xu,Y., Muto,A., Himeno,H., Deng,H., Lei,J. and Gao,N. (2013) Dissecting the in vivo assembly of the 30S ribosomal subunit reveals the role of RimM and general features of the assembly process. *Nucleic Acids Res.*, **41**, 2609–2620.
34. Naganathan,A. and Moore,S.D. (2013) Crippling the essential GTPase Der causes dependence on ribosomal protein L9. *J. Bacteriol.*, **195**, 3682–3691.
35. Li,N., Chen,Y., Guo,Q., Zhang,Y., Yuan,Y., Ma,C., Deng,H., Lei,J. and Gao,N. (2013) Cryo-EM structures of the late-stage assembly intermediates of the bacterial 50S ribosomal subunit. *Nucleic Acids Res.*, **41**, 7073–7083.
36. Schuwirth,B.S., Borovinskaya,M.A., Hau,C.W., Zhang,W., Vila-Sanjurjo,A., Holton,J.M. and Cate,J.H. (2005) Structures of the bacterial ribosome at 3.5 A resolution. *Science*, **310**, 827–834.
37. Rodnina,M.V., Stark,H., Savelsbergh,A., Wieden,H.J., Mohr,D., Matassova,N.B., Peske,F., Daviter,T., Gualerzi,C.O. and Wintermeyer,W. (2000) GTPases mechanisms and functions of translation factors on the ribosome. *Biol. Chem.*, **381**, 377–387.
38. Hwang,J. and Inouye,M. (2010) A bacterial GAP-like protein, YihI, regulating the GTPase of Der, an essential GTP-binding protein in Escherichia coli. *J. Mol. Biol.*, **399**, 759–772.
39. Wittinghofer,A. and Vetter,I.R. (2011) Structure-function relationships of the G domain, a canonical switch motif. *Annu. Rev. Biochem.*, **80**, 943–971.
40. Gasper,R., Meyer,S., Gotthardt,K., Sirajuddin,M. and Wittinghofer,A. (2009) It takes two to tango: regulation of G proteins by dimerization. *Nat. Rev. Mol. Cell Biol.*, **10**, 423–429.
41. Egea,P.F., Shan,S.O., Napetschnig,J., Savage,D.F., Walter,P. and Stroud,R.M. (2004) Substrate twinning activates the signal recognition particle and its receptor. *Nature*, **427**, 215–221.
42. Scrima,A. and Wittinghofer,A. (2006) Dimerisation-dependent GTPase reaction of MnmE: how potassium acts as GTPase-activating element. *EMBO J.*, **25**, 2940–2951.
43. Bugl,H., Fauman,E.B., Staker,B.L., Zheng,F., Kushner,S.R., Saper,M.A., Bardwell,J.C. and Jakob,U. (2000) RNA methylation under heat shock control. *Mol. Cell*, **6**, 349–360.
44. Caldas,T., Binet,E., Bouloc,P. and Richarme,G. (2000) Translational defects of Escherichia coli mutants deficient in the Um(2552) 23S ribosomal RNA methyltransferase RrmJ/FTSJ. *Biochem. Biophys. Res. Commun.*, **271**, 714–718.
45. Sharma,M.R., Barat,C., Wilson,D.N., Booth,T.M., Kawazoe,M., Hori-Takemoto,C., Shirouzu,M., Yokoyama,S., Fucini,P. and Agrawal,R.K. (2005) Interaction of Era with the 30S ribosomal subunit implications for 30S subunit assembly. *Mol. Cell*, **18**, 319–329.
46. Datta,P.P., Wilson,D.N., Kawazoe,M., Swami,N.K., Kaminishi,T., Sharma,M.R., Booth,T.M., Takemoto,C., Fucini,P., Yokoyama,S. *et al.* (2007) Structural aspects of RbfA action during small ribosomal subunit assembly. *Mol. Cell*, **28**, 434–445.
47. Feng,B., Mandava,C.S., Guo,Q., Wang,J., Cao,W., Li,N., Zhang,Y., Zhang,Y., Wang,Z., Wu,J. *et al.* (2014) Structural and functional insights into the maction of a universally conserved Obg GTPase. *PLoS Biol.*, **12**, e1001866.
48. Guo,Q., Yuan,Y., Xu,Y., Feng,B., Liu,L., Chen,K., Sun,M., Yang,Z., Lei,J. and Gao,N. (2011) Structural basis for the function of a small GTPase RsgA on the 30S ribosomal subunit maturation revealed by cryoelectron microscopy. *Proc. Natl. Acad. Sci. U.S.A.*, **108**, 13100–13105.
49. Boehringer,D., O'Farrell,H.C., Rife,J.P. and Ban,N. (2012) Structural insights into methyltransferase KsgA function in 30S ribosomal subunit biogenesis. *J. Biol. Chem.*, **287**, 10453–10459.
50. Chen,B., Boel,G., Hashem,Y., Ning,W., Fei,J., Wang,C., Gonzalez,R.L. Jr., Hunt,J.F. and Frank,J. (2014) EttA regulates translation by binding the ribosomal E site and restricting ribosome-tRNA dynamics. *Nat. Struct. Mol. Biol.*, **21**, 152–159.
51. Boel,G., Smith,P.C., Ning,W., Englander,M.T., Chen,B., Hashem,Y., Testa,A.J., Fischer,J.J., Wieden,H.J., Frank,J. *et al.* (2014) The ABC-F protein EttA gates ribosome entry into the translation elongation cycle. *Nat. Struct. Mol. Biol.*, **21**, 143–151.
52. Hwang,J. and Inouye,M. (2008) RelA functionally suppresses the growth defect caused by a mutation in the G domain of the essential Der protein. *J. Bacteriol.*, **190**, 3236–3243.
53. Lee,R., Aung-Htut,M.T., Kwik,C. and March,P.E. (2011) Expression phenotypes suggest that Der participates in a specific, high affinity interaction with membranes. *Protein Expr. Purif.*, **78**, 102–112.
54. Morimoto,T., Loh,P.C., Hirai,T., Asai,K., Kobayashi,K., Moriya,S. and Ogasawara,N. (2002) Six GTP-binding proteins of the Era/Obg family are essential for cell growth in Bacillus subtilis. *Microbiol.*, **148**, 3539–3552.
55. Dalebroux,Z.D. and Swanson,M.S. (2012) ppGpp: magic beyond RNA polymerase. *Nat. Rev. Microbiol.*, **10**, 203–212.
56. Mitkevich,V.A., Ermakov,A., Kulikova,A.A., Tankov,S., Shyp,V., Soosaar,A., Tenson,T., Makarov,A.A., Ehrenberg,M. and Hauryliuk,V. (2010) Thermodynamic characterization of ppGpp binding to EF-G or IF2 and of initiator tRNA binding to free IF2 in the presence of GDP, GTP, or ppGpp. *J. Mol. Biol.*, **402**, 838–846.